Evaluation of longitudinal double-spin asymmetry measurements in semi-inclusive deep-inelastic scattering from the proton for the ECCE detector design

C. Van Hulse [22,63,*], J.K. Adkins [33], Y. Akiba [50,54], A. Albataineh [69], M. Amaryan [44], I.C. Arsene [73], C. Ayerbe Gayoso [35], J. Bae [59], X. Bai [80], M.D. Baker [5,27], M. Bashkanov [89], R. Bellwied [67], F. Benmokhtar [15], V. Berdnikov [13], J.C. Bernauer [52,53,54], F. Bock [46], W. Boeglin [16], M. Borysova [84], E. Brash [11], P. Brindza [27], W.J. Briscoe [20], M. Brooks [30], S. Bueltmann [44], M.H.S. Bukhari [26], A. Bylinkin [69], R. Capobianco [65], W.-C. Chang [2], Y. Cheon [57], K. Chen [8], K.-F. Chen [43], K.-Y. Cheng [37], M. Chiu [5], T. Chujo [77], Z. Citron [4], E. Cline [52,53], E. Cohen [41], T. Cormier [46,a], Y. Corrales Morales [30], C. Cotton [80], J. Crafts [13], C. Crawford [70], S. Creekmore [46], C.Cuevas [27], J. Cunningham [46], G. David [5], C.T. Dean [30], M. Demarteau [46], S. Diehl [65], N. Doshita [86], R. Dupré [22], J.M. Durham [30], R. Dzhygadlo [19], R. Ehlers [46], L. El Fassi [35], A. Emmert [80], R. Ent [27], C. Fanelli [34,85,27], R. Fatemi [70], S. Fegan [89], M. Finger [9], M. Finger Jr. [9], J. Frantz [45], M. Friedman [21], I. Friscic [34,27], D. Gangadharan [67], S. Gardner [18], K. Gates [18], F. Geurts [49], R. Gilman [51], D. Glazier [18], E. Glimos [46,79], Y. Goto [50,54], N. Grau [3], S.V. Greene [81], A.Q. Guo [24], L. Guo [16], S.K. Ha [87], J. Haggerty [5], T. Hayward [65], X. He [17], O. Hen [34], D.W. Higinbotham [27], M. Hoballah [22], T. Horn [13], A. Hoghmrtsyan [1], P.-h.J. Hsu [42], J. Huang [5], G. Huber [74], A. Hutson [67], K.Y. Hwang [88], C.E. Hyde [44], M. Inaba [62], T. Iwata [86], H.S. Jo [29], K. Joo [65], N. Kalantarians [82], G. Kalicy [13], K. Kawade [58], S.J.D. Kay [74], A. Kim [65], B. Kim [59], C. Kim [48], M. Kim [50], Y. Kim [48], Y. Kim [57], E. Kistenev [5], V. Klimenko [65], S.H. Ko [56], I. Korover [34], W. Korsch [70], G. Krintiras [69], S. Kuhn [44], C.-M. Kuo [37], T. Kutz [34], J. Lajoie [25], D. Lawrence [27], S. Lebedev [25], H. Lee [59], J.S.H. Lee [76], S.W. Lee [29], Y.-J. Lee [34], W. Li [49], W.B. Li [52,53,85], X. Li [75], X. Li [10], X. Li [30], X. Li [34], Y.T. Liang [24], S. Lim [48], C.-H. Lin [2], D.X. Lin [24], K. Liu [30], M.X. Liu [30], K. Livingston [18], N. Liyanage [80], W.J. Llope [83], C. Loizides [46], E. Long [72], R.-S. Lu [43], Z. Lu [10], W. Lynch [89], S. Mantry [66], D. Marchand [22], M. Marcisovsky [14], C. Markert [78], P. Markowitz [16], H. Marukyan [1], P. McGaughey [30], M. Mihovilovic [71], R.G. Milner [34], A. Milov [84], Y. Miyachi [86], A. Mkrtchyan [1], H. Mkrtchyan [1], P. Monaghan [11], R. Montgomery [18], D. Morrison [5], A. Movsisyan [1], C. Munoz Camacho [22], M. Murray [69], K. Nagai [30], J. Nagle [64], I. Nakagawa [50], C. Nattrass [79], D. Nguyen [27], S. Niccolai [22], R. Nouicer [5], G. Nukazuka [50], M. Nycz [80], V.A. Okorokov [40], S. Orešić [74], J.D. Osborn [46], C. O'Shaughnessy [30], S. Paganis [43], Z. Papandreou [74], S.F. Pate [39], M. Patel [25], C. Paus [34], G. Penman [18], M.G. Perdekamp [68], D.V. Perepelitsa [64], H. Periera da Costa [30], K. Peters [19], W. Phelps [11], E. Piasetzky [60], C. Pinkenburg [5], I. Prochazka [9], T. Protzman [31], M.L. Purschke [5], J. Putschke [83], J.R. Pybus [34], R. Rajput-Ghoshal [27], J. Rasson [46], K.F. Read [46,79], K. Røed [73], R. Reed [31], J. Reinhold [16], E.L. Renner [30], J. Richards [65], C. Riedl [68], T. Rinn [5], J. Roche [45], G.M. Roland [34], G. Ron [21], M. Rosati [25], C. Royon [69], J. Ryu [48], S. Salur [51], N. Santiesteban [34], R. Santos [65], M. Sarsour [17], J. Schambach [46], A. Schmidt [20], N. Schmidt [46],

* Corresponding author at: Universidad de Alcala, Alcala de Henares, Madrid, Spain.
  E-mail address: cvanhuls@mail.cern.ch (C. Van Hulse).
  a Deceased.

C. Schwarz [19], J. Schwiening [19], R. Seidl [50,54], A. Sickles [68], P. Simmerling [65], S. Sirca [71], D. Sharma [17], Z. Shi [30], T.-A. Shibata [38], C.-W. Shih [37], S. Shimizu [50], U. Shrestha [65], K. Slifer [72], K. Smith [30], D. Sokhan [18,23], R. Soltz [32], W. Sondheim [30], J. Song [10], J. Song [48], I.I. Strakovsky [20], P. Steinberg [5], P. Stepanov [13], J. Stevens [85], J. Strube [47], P. Sun [10], X. Sun [8], K. Suresh [74], V. Tadevosyan [1], W.-C. Tang [37], S. Tapia Araya [25], S. Tarafdar [81], L. Teodorescu [6], D. Thomas [78], A. Timmins [67], L. Tomasek [14], N. Trotta [65], R. Trotta [13], T.S. Tveter [73], E. Umaka [25], A. Usman [74], H.W. van Hecke [30], J. Velkovska [81], E. Voutier [22], P.K. Wang [22], Q. Wang [69], Y. Wang [8], Y. Wang [61], D.P. Watts [89], N. Wickramaarachchi [13], L. Weinstein [44], M. Williams [34], C.-P. Wong [30], L. Wood [47], M.H. Wood [7], C. Woody [5], B. Wyslouch [34], Z. Xiao [61], Y. Yamazaki [28], Y. Yang [36], Z. Ye [61], H.D. Yoo [88], M. Yurov [30], N. Zachariou [89], W.A. Zajc [12], W. Zha [75], J.-L. Zhang [55], J.-X. Zhang [80], Y. Zhang [61], Y.-X. Zhao [24], X. Zheng [80], P. Zhuang [61]

[1] *A. Alikhanyan National Laboratory, Yerevan, Armenia*
[2] *Institute of Physics, Academia Sinica, Taipei, Taiwan*
[3] *Augustana University, Sioux Falls, SD, USA*
[4] *Ben-Gurion University of the Negev, Beer-Sheva, Israel*
[5] *Brookhaven National Laboratory, Upton, NY, USA*
[6] *Brunel University London, Uxbridge, UK*
[7] *Canisius College, Buffalo, NY, USA*
[8] *Central China Normal University, Wuhan, China*
[9] *Charles University, Prague, Czech Republic*
[10] *China Institute of Atomic Energy, Fangshan, Beijing, China*
[11] *Christopher Newport University, Newport News, VA, USA*
[12] *Columbia University, New York, NY, USA*
[13] *Catholic University of America, Washington DC, USA*
[14] *Czech Technical University, Prague, Czech Republic*
[15] *Duquesne University, Pittsburgh, PA, USA*
[16] *Florida International University, Miami, FL, USA*
[17] *Georgia State University, Atlanta, GA, USA*
[18] *University of Glasgow, Glasgow, UK*
[19] *GSI Helmholtzzentrum fuer Schwerionenforschung GmbH, Darmstadt, Germany*
[20] *The George Washington University, Washington, DC, USA*
[21] *Hebrew University, Jerusalem, Isreal*
[22] *Universite Paris-Saclay, CNRS/IN2P3, IJCLab, Orsay, France*
[23] *IRFU, CEA, Universite Paris-Saclay, Gif-sur-Yvette, France*
[24] *Chinese Academy of Sciences, Lanzhou, China*
[25] *Iowa State University, Iowa City, IA, USA*
[26] *Jazan University, Jazan, Sadui Arabia*
[27] *Thomas Jefferson National Accelerator Facility, Newport News, VA, USA*
[28] *Kobe University, Kobe, Japan*
[29] *Kyungpook National University, Daegu, Republic of Korea*
[30] *Los Alamos National Laboratory, Los Alamos, NM, USA*
[31] *Lehigh University, Bethlehem, PA, USA*
[32] *Lawrence Livermore National Laboratory, Livermore, CA, USA*
[33] *Morehead State University, Morehead, KY, USA*
[34] *Massachusetts Institute of Technology, Cambridge, MA, USA*
[35] *Mississippi State University, Mississippi State, MS, USA*
[36] *National Cheng Kung University, Tainan, Taiwan*
[37] *National Central University, Chungli, Taiwan*
[38] *Nihon University, Tokyo, Japan*
[39] *New Mexico State University, Las Cruces, NM, USA*
[40] *National Research Nuclear University MEPhI, Moscow, Russian Federation*
[41] *Nuclear Research Center - Negev, Beer-Sheva, Isreal*
[42] *National Tsing Hua University, Hsinchu, Taiwan*
[43] *National Taiwan University, Taipei, Taiwan*
[44] *Old Dominion University, Norfolk, VA, USA*
[45] *Ohio University, Athens, OH, USA*
[46] *Oak Ridge National Laboratory, Oak Ridge, TN, USA*
[47] *Pacific Northwest National Laboratory, Richland, WA, USA*
[48] *Pusan National University, Busan, Republic of Korea*
[49] *Rice University, Houston, TX, USA*
[50] *RIKEN Nishina Center, Wako, Saitama, Japan*
[51] *The State University of New Jersey, Piscataway, NJ, USA*
[52] *Center for Frontiers in Nuclear Science, Stony Brook, NY, USA*
[53] *Stony Brook University, Stony Brook, NY, USA*
[54] *RIKEN BNL Research Center, Upton, NY, USA*
[55] *Shandong University, Qingdao, Shandong, China*
[56] *Seoul National University, Seoul, Republic of Korea*
[57] *Sejong University, Seoul, Republic of Korea*
[58] *Shinshu University, Matsumoto, Nagano, Japan*
[59] *Sungkyunkwan University, Suwon, Republic of Korea*
[60] *Tel Aviv University, Tel Aviv, Israel*
[61] *Tsinghua University, Beijing, China*
[62] *Tsukuba University of Technology, Tsukuba, Ibaraki, Japan*

[63] *Universidad de Alcala, Alcala de Henares, Madrid, Spain*
[64] *University of Colorado Boulder, Boulder, CO, USA*
[65] *University of Connecticut, Storrs, CT, USA*
[66] *University of North Georgia, Dahlonega, GA, USA*
[67] *University of Houston, Houston, TX, USA*
[68] *University of Illinois, Urbana, IL, USA*
[69] *University of Kansas, Lawrence, KS, USA*
[70] *University of Kentucky, Lexington, KY, USA*
[71] *University of Ljubljana, Ljubljana, Slovenia*
[72] *University of New Hampshire, Durham, NH, USA*
[73] *University of Oslo, Oslo, Norway*
[74] *University of Regina, Regina, SK, Canada*
[75] *University of Science and Technology of China, Hefei, China*
[76] *University of Seoul, Seoul, Republic of Korea*
[77] *University of Tsukuba, Tsukuba, Japan*
[78] *University of Texas, Austin, TX, USA*
[79] *University of Tennessee, Knoxville, TN, USA*
[80] *University of Virginia, Charlottesville, VA, USA*
[81] *Vanderbilt University, Nashville, TN, USA*
[82] *Virginia Union University, Richmond, VA, USA*
[83] *Wayne State University, Detroit, MI, USA*
[84] *Weizmann Institute of Science, Rehovot, Israel*
[85] *The College of William and Mary, Williamsburg, VA, USA*
[86] *Yamagata University, Yamagata, Japan*
[87] *Yarmouk University, Irbid, Jordan*
[88] *Yonsei University, Seoul, Republic of Korea*
[89] *University of York, York, UK*

ARTICLE INFO

ABSTRACT

The evaluation of the measurement of double-spin asymmetries for charge-separated pions and kaons produced in deep-inelastic scattering from the proton using the ECCE detector design concept is presented, for the combinations of lepton and hadron beam energies of 5×41 GeV^2 and 18×275 GeV^2. The study uses unpolarised simulated data that are processed through a full GEANT simulation of the detector. These data are then reweighted at the parton level with DSSV helicity distributions and DSS fragmentation functions, in order to generate the relevant asymmetries, and subsequently analysed. The performed analysis shows that the ECCE detector concept provides the resolution and acceptance, with a broad coverage in kinematic phase space, needed for a robust extraction of asymmetries. This, in turn, allows for a precise extraction of sea-quark helicity distributions.

Contents

1. Introduction

The measurement of the longitudinal double-spin asymmetry in deep-inelastic scattering (DIS) provides an experimentally clean access to the helicity parton distribution functions (PDFs). The asymmetry is proportional to the sum of convolutions of helicity distributions and fragmentation functions, where the convolutions are weighted by the charge squared of the parton struck in the DIS process. Through the measurement of asymmetries in semi-inclusive DIS, where the formed hadron is tagged, one gains sensitivity to the parton flavour. The combined analysis of existing measurements of longitudinal double-spin asymmetries in inclusive and semi-inclusive DIS as well as in proton–proton collisions already provides constraints on parton helicity distributions at moderate Bjorken-x, x_B [1]. Yet, because of absence of data, the sea-quark and gluon helicity distributions, at lower values of x_B, suffer from large uncertainties. The measurement of inclusive DIS at the Electron-Ion Collider (EIC) is expected to provide strong constraints

on the gluon helicity distribution at low x_B, since the large Q^2 coverage of the EIC allows one to probe Q^2 evolution, while the strength of semi-inclusive measurements at an EIC lies in the determination of the individual sea-quark helicity distributions. The expected performance of the EIC Comprehensive Chromodynamics Experiment (ECCE) detector for the measurement of longitudinal double-spin asymmetries in the production of charge-separated pions and kaons in semi-inclusive DIS is evaluated through the study of a Monte-Carlo simulation. The result of this study is presented in this note.

In Section 2, the used Monte-Carlo simulations as well as the data selection are described. In Section 3, the asymmetries extracted from the Monte-Carlo simulation are presented, while in Section 4 the impact of the foreseen measurements on the helicity distributions are shown. Finally, in Section 5, the conclusions are summarised.

2. Data selection and Monte-Carlo reweighting

The semi-inclusive DIS events are generated with the PYTHIA-6 [2] (eRHIC) Monte-Carlo simulation, using the same steering-card settings
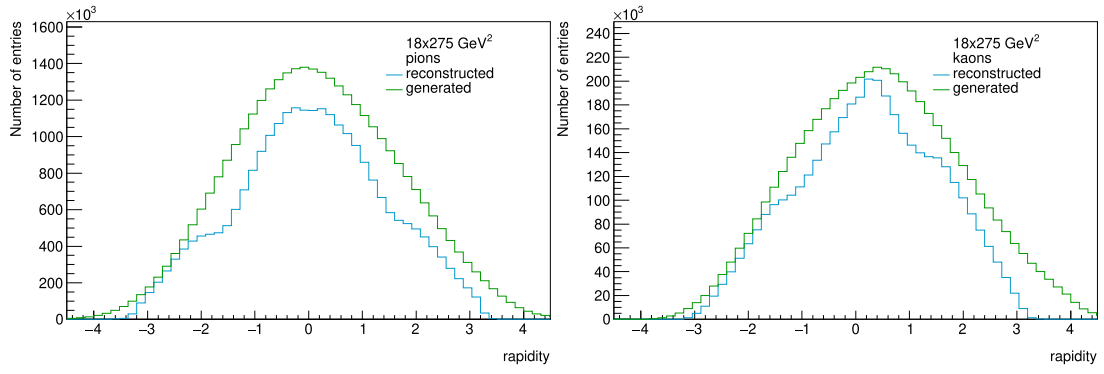
Fig. 1. Rapidity distribution (in the laboratory frame) of generated (green line) and reconstructed (blue line) pions (left) and kaons (right).

Table 1
Luminosity of the various Monte-Carlo data sets, generated at the energy configurations 18×275 GeV^2 and 5×41 GeV^2.

	$Q^2 > 1$ GeV^2	1 GeV$^2 < Q^2 < 100$ GeV^2	$Q^2 > 100$ GeV^2
18×275 GeV^2	21.923 pb^{-1}	21.995 pb^{-1}	1231.564 pb^{-1}
5×41 GeV^2	61.402 pb^{-1}	61.483 pb^{-1}	5944.374 pb^{-1}

Table 2
Used kinematic bins in x_B, Q^2, and z.

x_B	1.0e−05	1.58489e−05	2.51189e−05	3.98107e−05	6.30957e−05
	1.0e−04	1.58489e−04	2.51189e−04	3.98107e−04	6.30957e−04
	1.0e−03	1.58489e−03	2.51189e−03	3.98107e−03	6.30957e−03
	1.0e−02	1.58489e−02	2.51189e−02	3.98107e−02	6.30957e−02
	1.0e−01	1.58489e−01	2.51189e−01	3.98107e−01	6.30957e−01
	1.0				
Q^2 [GeV^2]	1.0	1.77828	3.16228	5.62341	
	10.0	17.7828	31.6228	56.2341	
	100.0	177.828	316.228	562.341	
	1000.0	10000.0			
z	0.01	0.05	0.10	0.15	0.20
	0.25	0.30	0.40	0.50	0.60
	0.70	0.80	0.90	1.00	

as those used for the Yellow Report [3]. Only the default PYTHIA initial-state and final-state radiation are included in this simulation, while dedicated radiative effects are absent. Radiative effects present in measurements can be evaluated through unfolding techniques using dedicated Monte-Carlo simulations. The generated output is passed through a full GEANT simulation of the ECCE detector. The detector configuration of the second simulation campaign, i.e., the 'July concept' [4], is used to produce and reconstruct the simulated data for the here presented studies. Unless stated otherwise, the field strength of the ECCE solenoid superconducting magnet is set to 1.4 T.

Since the PYTHIA-6 Monte Carlo does not include helicity distributions, the simulated data needs to be reweighted.[1] The applied weights are evaluated at next-to-leading order in perturbative QCD, at the generated values of the kinematic variables x_B, $Q^2 = -q^2$, and $z = (p \cdot P_h)/(p \cdot q)$, where q, p, and P_h represent the four momenta of, respectively, the virtual photon, beam proton and created hadron. The weights are of the form

$$1 + \lambda D(y) \frac{\Delta \otimes D^{q,g \to h}}{F_{UU}^h}, \quad (1)$$

where $\lambda = +1$ or $\lambda = -1$ depending if the beam lepton and beam proton have their spin orientation respectively parallel or anti-parallel. The respective orientation of the spin of the lepton and proton beams is for each event randomly simulated. The depolarisation factor is represented by $D(y)$, where y is the inelasticity. The depolarisation

---

[1] Only the processes with PYTHIA ID 99 and 131–136 are reweighted.

factor depends on the ratio of the longitudinal-to-transverse virtual-photon absorption cross sections. For the evaluation of this ratio, the parameterisation from Ref. [5] is used. The term Δ stands for $e_q^2 \Delta q$, with e_q^2 the parton charge squared and Δq the quark helicity PDF, or Δg, the gluon helicity PDF, depending if the primary, struck parton is a quark or a gluon. The symbol $\otimes$ represents the convolution integral of the parton helicity distribution and the fragmentation function, $D^{q,g \to h}$, evaluated at next-to-leading order. As input, the DSSV14 helicity distributions [1, 6] and the DSS14 pion and kaon fragmentation functions [7,8] are used. The unpolarised structure function F_{UU}^h is the (charge-squared) weighted sum of the convolution integrals of the spin-independent PDFs and fragmentation functions. For the PDFs, the NNPDF30_nlo_as_0118 set [9], evaluated through the LHAPDF interpolator [10], is used. The next-to-leading order semi-inclusive DIS coefficients needed in the calculation are taken from Ref. [11].
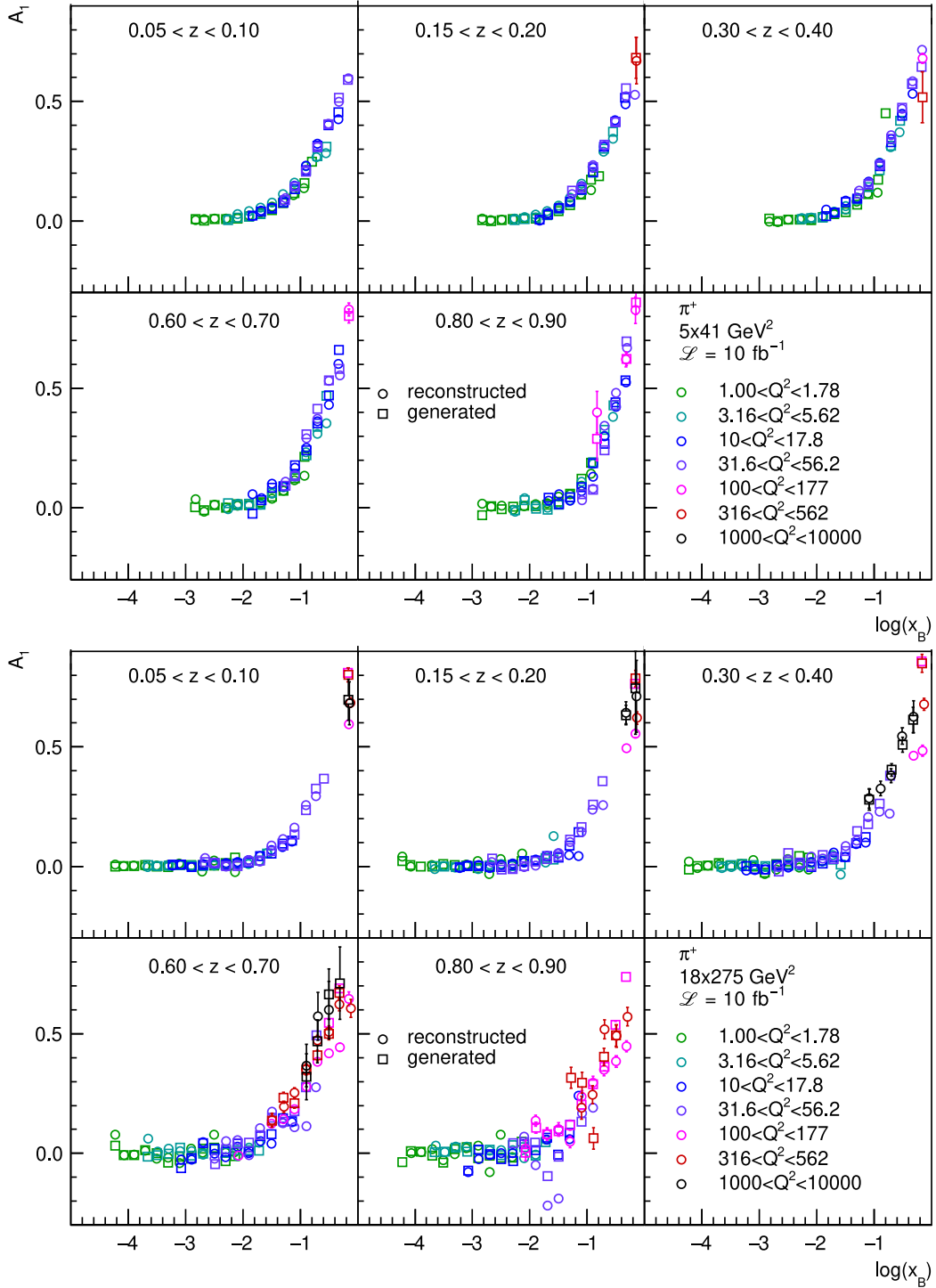
Data have been simulated for various sets of lepton and proton beam energies: 5 GeV and 41 GeV, 10 GeV and 100 GeV, 18 GeV and 100 GeV, and 18 GeV and 275 GeV. In order to illustrate the impact of the ECCE design on the determination of the helicity distributions, the studies for data simulated at the highest and lowest centre-of-mass energies, $\sqrt{s}$, are presented. For these energies, the simulated data sets, generated for different regions in Q^2, and their corresponding luminosity are summarised in Table 1. In the present study, the statistical uncertainties of the asymmetries are scaled to an integrated luminosity of 10 fb^{-1}.

For the evaluation of the double-spin asymmetries, events satisfying the following criteria are selected: $Q^2 > 1$ GeV^2, in order to be in the DIS regime, a squared invariant mass of the photon-nucleon system $W^2 > 10$ GeV^2, in order to avoid the region dominated by baryon-resonance production, and an inelasticity $0.01 < y < 0.95$, where the upper cut aims at limiting contributions from QED radiation and the lower cut removes events with a degraded resolution in the particle's momentum reconstruction. The (reconstructed) hadrons are identified using the generated Monte-Carlo information and their fractional energy with respect to the energy of the virtual photon exchanged in the lepton-proton interaction, z, is restricted to lie above 0.01, in order to limit contributions from target fragmentation. No special requirement is placed on the hadron rapidity. The rapidity distribution (in the laboratory frame) of the generated and reconstructed pions and kaons is presented in Fig. 1. The selected data sample is evaluated in 25 bins of x_B, 13 bins of Q^2, and 13 bins of z, as presented in Table 2.

3. Evaluation of the asymmetries

Experimentally clean access in semi-inclusive DIS to the helicity distributions is provided by the extraction of longitudinal double-spin asymmetries. Assuming constant lepton-beam and proton-beam

Fig. 2. Generated (squares) and reconstructed (circles) double-spin asymmetries with $D(y) = 1$ for positive pions, as a function of x_B and for selected ranges in z (panels) and Q^2 (colours). The data points are drawn at, respectively, the average generated and average reconstructed x_B in each bin. The data are generated at 5×41 GeV^2 (top two rows) and 18×275 GeV^2 (bottom two rows) and scaled to an integrated luminosity of 10 fb^{-1}.
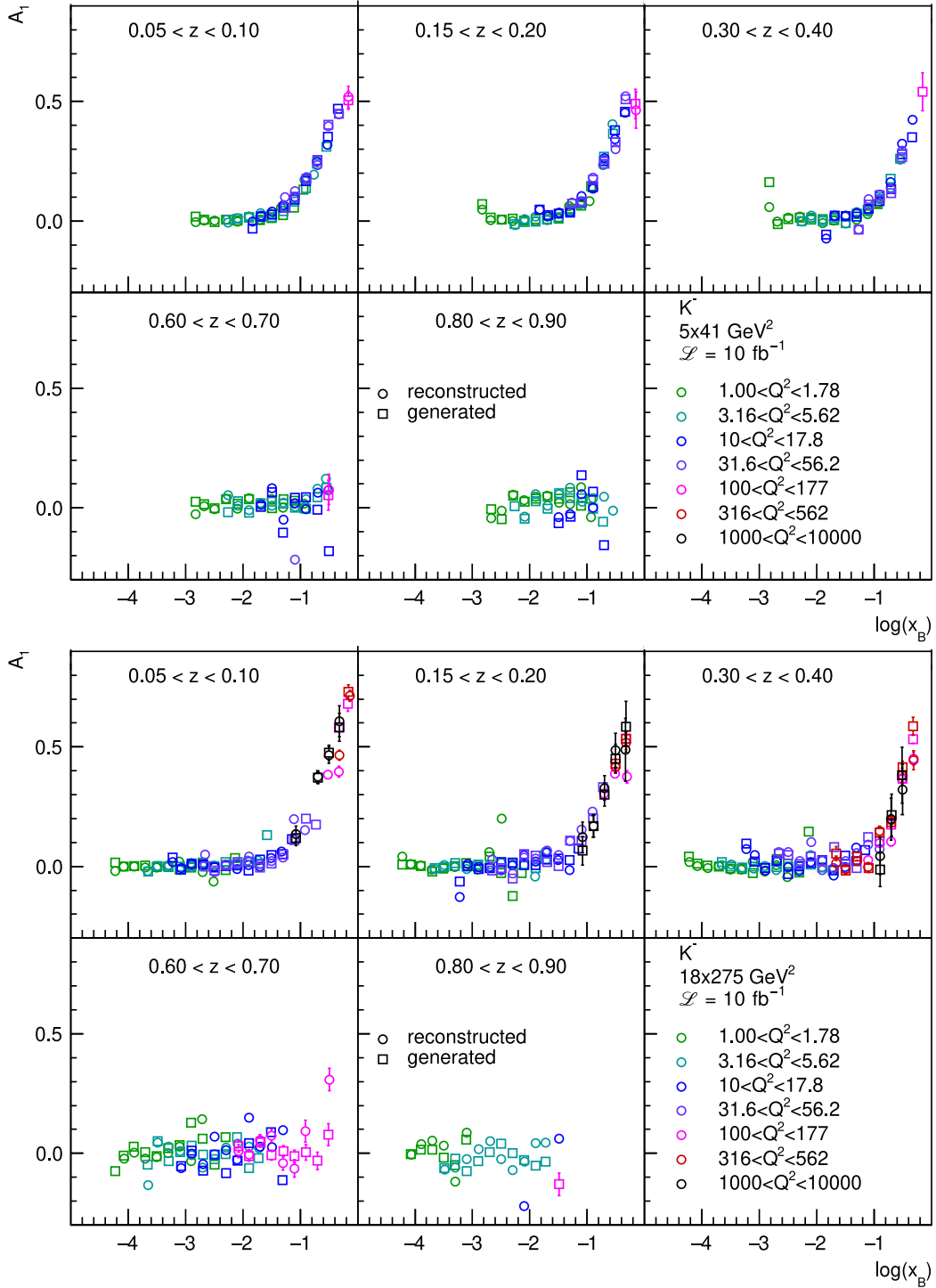
polarisation, respectively P_e and P_p, they can be written as:

$$A_\parallel^h(x_B, Q^2, z) = \frac{1}{P_e P_p} \frac{\frac{\overrightarrow{\overrightarrow{N^h}}}{\overrightarrow{\overrightarrow{L}}} - \frac{\overrightarrow{\overleftarrow{N^h}}}{\overrightarrow{\overleftarrow{L}}}}{\frac{\overrightarrow{\overrightarrow{N^h}}}{\overrightarrow{\overrightarrow{L}}} + \frac{\overrightarrow{\overleftarrow{N^h}}}{\overrightarrow{\overleftarrow{L}}}}(x_B, Q^2, z) \qquad (2)$$

$$= D(y) A_1^h(x_B, Q^2, z), \qquad (3)$$

where $\overrightarrow{\overrightarrow{N^h}}$ ($\overrightarrow{\overleftarrow{N^h}}$) represents the number of semi-inclusive DIS hadrons of type h in bin (x_B, Q^2, z) collected with (anti-)parallel beam-spin orientation, while $\overrightarrow{\overrightarrow{L}}$ ($\overrightarrow{\overleftarrow{L}}$) is the corresponding luminosity. The asymmetry $A_\parallel^h$ represents the asymmetry with respect to the lepton-beam direction, while A_1^h is the asymmetry with respect to the virtual photon and gives access to the convolution of the parton helicity distributions and fragmentation functions.

In the present simulation, N^h is obtained by reweighting each event, as described in Section 2, while the randomly generated relative

Fig. 3. Generated (squares) and reconstructed (circles) double-spin asymmetries with $D(y) = 1$ for negative kaons, as a function of x_B and for selected ranges in z (panels) and Q^2 (colours). The data points are drawn at, respectively, the average generated and average reconstructed x_B in each bin. The data are generated at 5×41 GeV^2 (top two rows) and 18×275 GeV^2 (bottom two rows) and scaled to an integrated luminosity of 10 fb^{-1}.
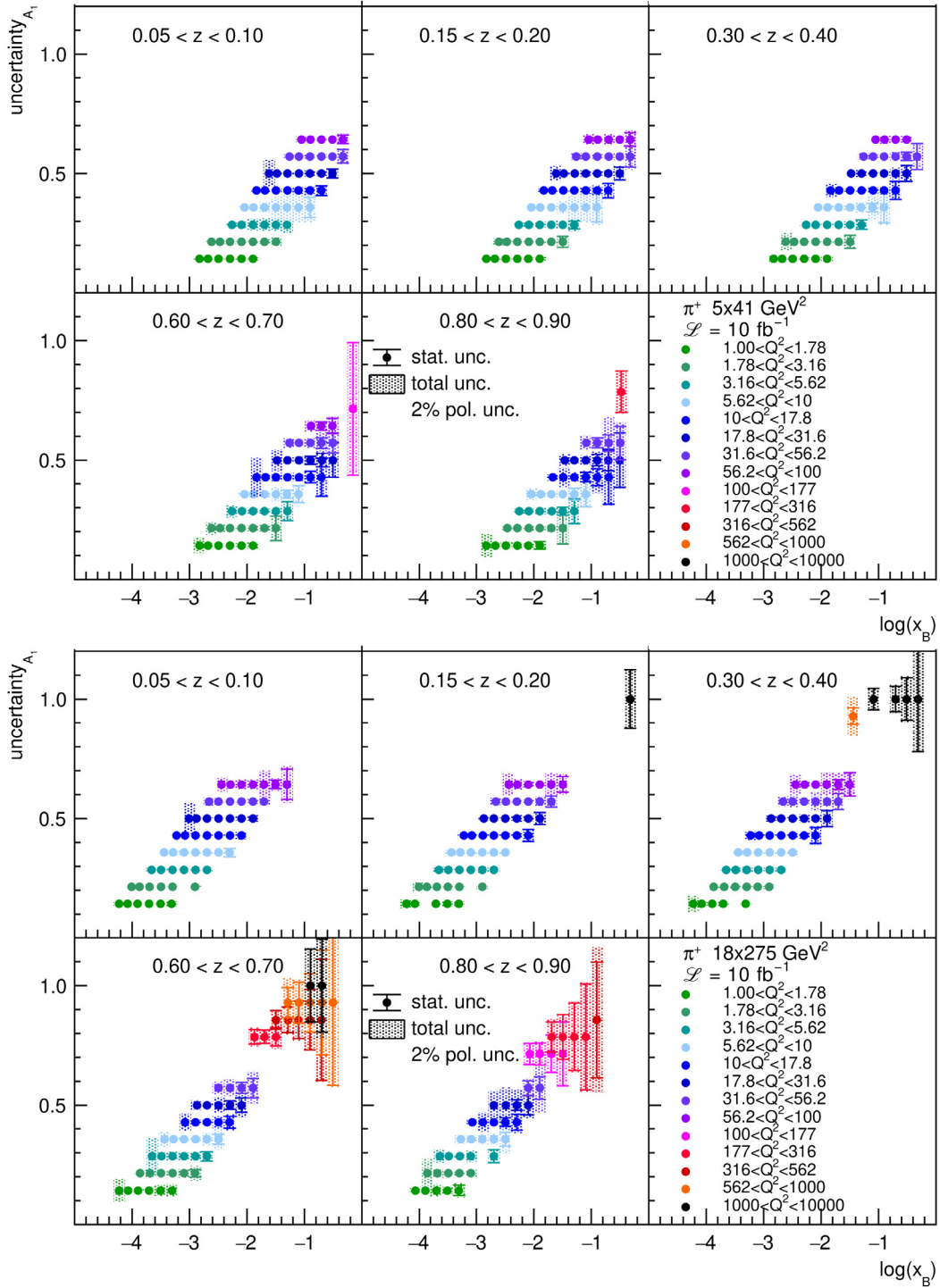
beam-spin orientation results in $\vec{\overline{L}} \approx \vec{\overline{\overline{L}}}$. The lepton and proton beam polarisations are set to 100% in the simulation, but in order to account for experimentally realistic conditions, a beam polarisation for both beams of 70% is assumed in the evaluation of the statistical uncertainty.

In the following, the depolarisation factor is set to 1 for the evaluation of the systematic uncertainties, both in Eq. (1) for the reweighting of the simulation and for the extraction of A_1 in Eq. (3). The reason for this approach lies in the enhancement of small differences between generated and reconstructed data points when introducing the

depolarisation factor due to fluctuations that result solely from the limited amount of generated Monte-Carlo data. For the evaluation of the statistical uncertainty, the actual value of the depolarisation factor is used in Eqs. (1) and (3) and in addition it is required to lie above 0.1.

The generated asymmetries, evaluated from the generated scattered beam-lepton and hadron information, as well as the reconstructed asymmetries, evaluated from the scattered beam lepton and created
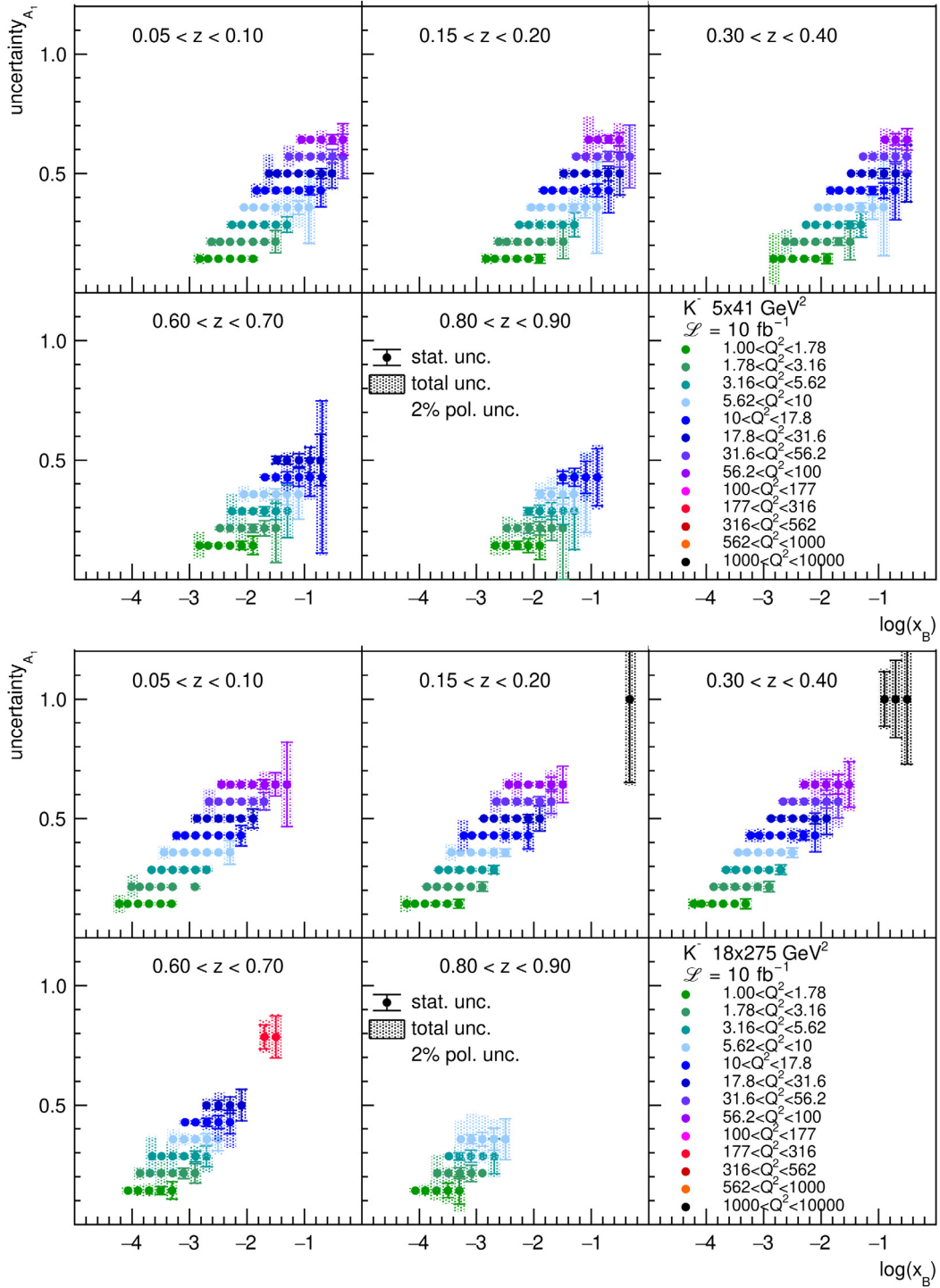
Fig. 4. Statistical (error bars) and total (error bands) uncertainty for each (x_B, Q^2) bin and for selected ranges in z, for positive-pion A_1 asymmetries at 5×41 GeV^2 (top two rows) and 18×275 GeV^2 (bottom two rows). An additional global scale uncertainty of 2% accounts for the uncertainty in the beam polarisations, as indicated in the figure. The central value on the vertical axis of the data points has no meaning.

particles reconstructed by the ECCE detector, based on tracking information only, are presented in Fig. 2 for positive pions and in Fig. 3 for negative kaons, for the beam-energy configurations 5×41 GeV^2 and 18×275 GeV^2. The depolarisation factor is set equal to 1 here. The different behaviour of the kaon and pion asymmetries at larger z values reflects the fact that, contrary to the pion, the negative kaon and the proton do not have a valence quark flavour in common. As can be seen from the figures, the reconstructed asymmetries agree quite well with the generated asymmetries, and any effect from unreconstructed

hadrons or smearing of the kinematic variables due to finite detector resolution stays very limited. In that sense, the ECCE design is robust and satisfies the requirements needed for the extraction of double-spin asymmetries.

The figures also clearly show the broad kinematic coverage in x_B, Q^2, and z, with the two centre-of-mass energies covering complementary regions in x_B for the different ranges in z. The data collected at high centre-of-mass energy allows one to reach x_B values down to 10^{-4}.

Fig. 5. Statistical (error bars) and total (error bands) uncertainty for each (x_B, Q^2) bin and for selected ranges in z, for negative-kaon A_1 asymmetries at 5×41 GeV^2 (top two rows) and 18×275 GeV^2 (bottom two rows). An additional global scale uncertainty of 2% accounts for the uncertainty in the beam polarisations, as indicated in the figure. The central value on the vertical axis of the data points has no meaning.

Such broad kinematic coverage is needed for a precise extraction of the various parton helicity distributions.

In a realistic experimental situation, an unfolding procedure would be applied to the measured asymmetry in order to extract the 'physics' asymmetry, free from detector effects. The application of such unfolding procedure in the present study would allow to extract a 'physics' asymmetry, which approaches the generated asymmetry more closely. Such unfolding would require a vastly larger sample of simulated data and an elaborate procedure, which surpasses the purpose of the present study. Instead, it is decided to take the difference between the generated and the reconstructed asymmetry as a systematic uncertainty in each kinematic (x_B, Q^2, z) bin. The corresponding, evaluated uncertainty is expected to constitute an upper limit on the systematic uncertainty. In addition to this systematic uncertainty, a global scale uncertainty of 2%, stemming from the uncertainty in each of the two beam polarisations, is taken into account.
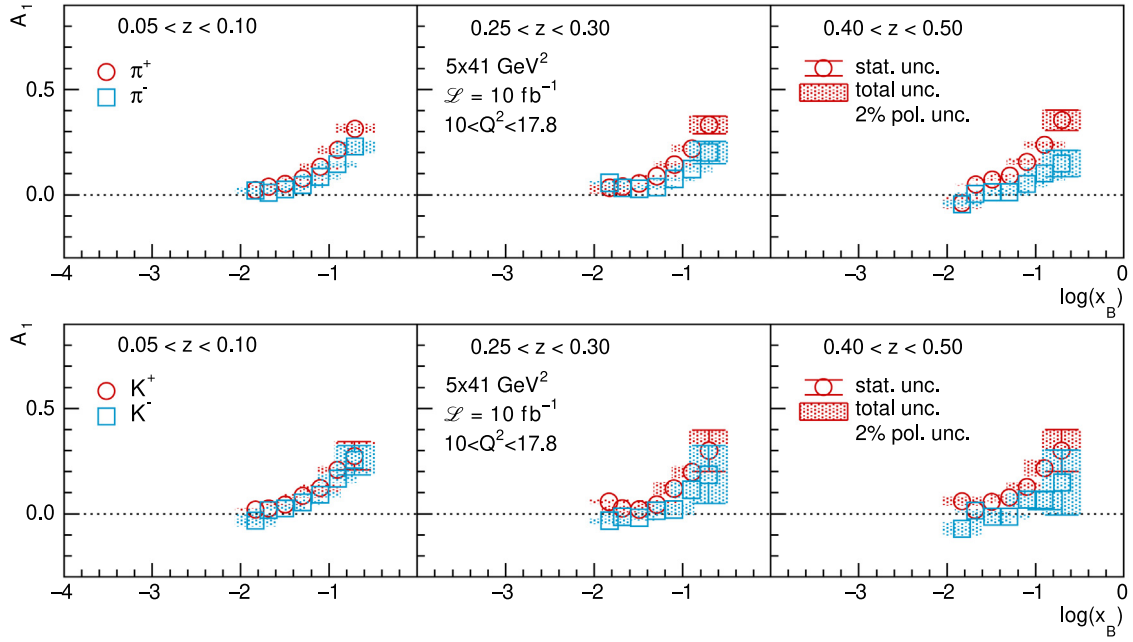
Fig. 6. 'Unfolded' pion (upper panel) and kaon (lower panel) A_1 asymmetries as a function of x_B for $10.0\ \text{GeV}^2 < Q^2 < 17.8\ \text{GeV}^2$ and three ranges in z, obtained from data at $5 \times 41\ \text{GeV}^2$ and for an integrated luminosity of $10\ \text{fb}^{-1}$.
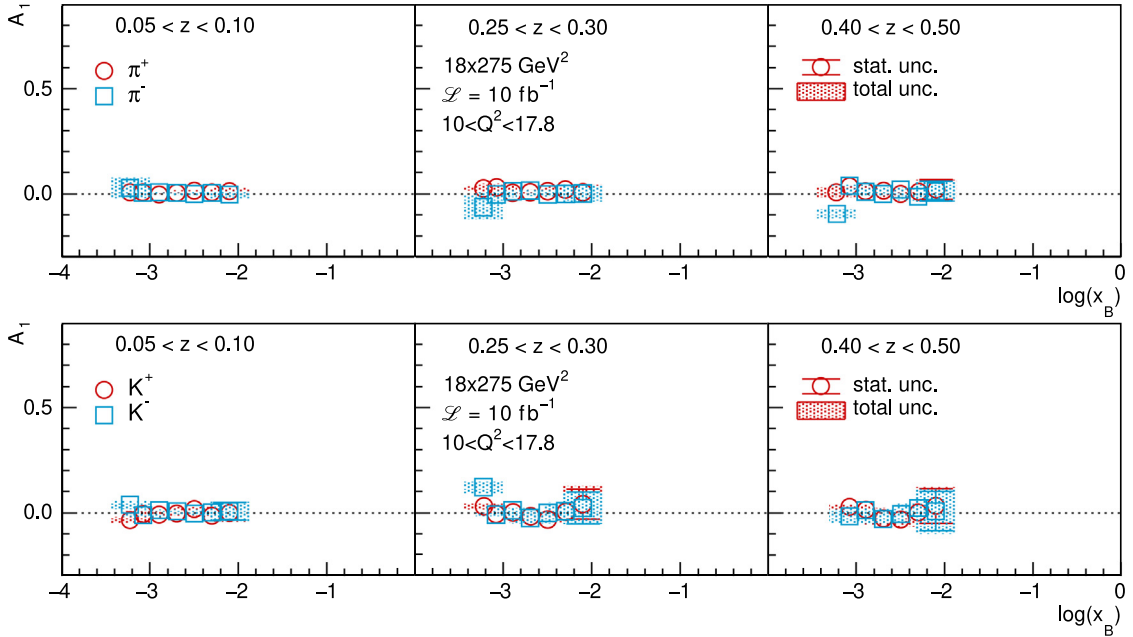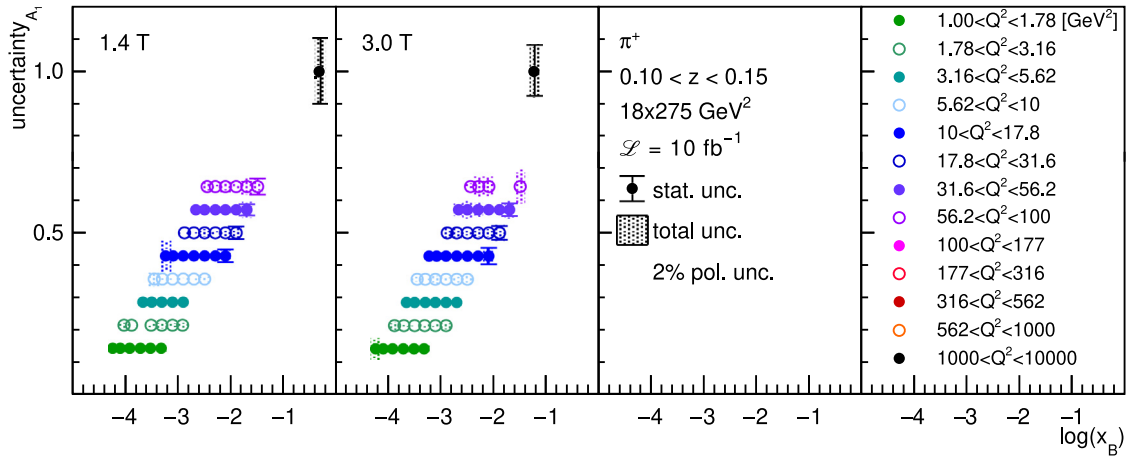

Fig. 7. 'Unfolded' pion (upper panel) and kaon (lower panel) A_1 asymmetries as a function of x_B for $10.0\ \text{GeV}^2 < Q^2 < 17.8\ \text{GeV}^2$ and three ranges in z, obtained from data at $18 \times 275\ \text{GeV}^2$ and for an integrated luminosity of $10\ \text{fb}^{-1}$.
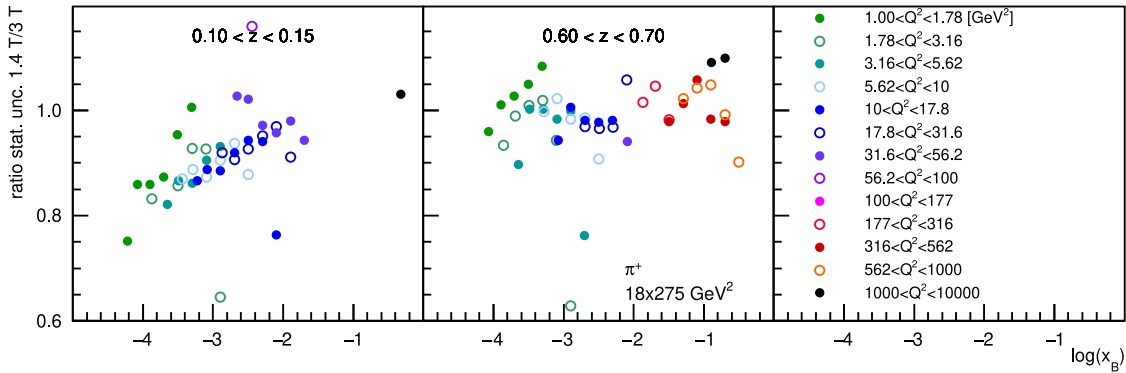
The statistical and systematic uncertainties on the A_1 asymmetry are summarised in Fig. 4 for positive pions and in Fig. 5 for negative kaons. The central value on the vertical axis is meaningless and only has been chosen for clear visibility. The error bars represent the statistical uncertainty (scaled to an integrated luminosity of $10\ \text{fb}^{-1}$ and accounting for beam polarisations of 70%), while the error band represents the combined systematic and statistical uncertainties. An additional 2% scale uncertainty originating from the uncertainty in the beam polarisations also needs to be included. On average, the systematic uncertainty is larger than the statistical uncertainty, yet, still very limited. The evaluation of the uncertainties shows that the ECCE detector design is suited to provide data with adequate precision.

Finally, Figs. 6 and 7 illustrate the asymmetry that would be obtained after an unfolding procedure on the asymmetry measured with the ECCE detector,[2] for $10\ \text{fb}^{-1}$ of data collected at $5 \times 41\ \text{GeV}^2$ and $18 \times 275\ \text{GeV}^2$, respectively, for the range $10.0\ \text{GeV}^2 < Q^2 < 17.8\ \text{GeV}^2$ and three ranges in z. The systematic uncertainties, evaluated as described above, are indicated as well. These figures again clearly illustrate the complementarity between data collected at the two centre-of-mass energies and their reach in x_B for a fixed range in z.

---

[2] In practice, the central values of the reconstructed asymmetries have been replaced here by those of the generated ones, for the kinematic bins for which an asymmetry is reconstructed.

Fig. 8. Statistical (error bars) and total (error bands) uncertainty for each (x_B, Q^2) bin and $0.10 < z < 0.15$, for positive-pion A_1 asymmetries at 18×275 GeV^2. An additional global scale uncertainty of 2% accounts for the uncertainty in the beam polarisations, as indicated in the figure. The central value on the vertical axis of the data points has no meaning. The first panel shows the kinematic coverage and related uncertainties with the 1.4 T magnet configuration, while the second panel shows the 3.0 T configuration.

Fig. 9. Ratio of the statistical uncertainties for positive-pion A_1 asymmetries at 18×275 GeV^2 with the 1.4 T and 3.0 T configurations, as a function of x_B (x axis) and Q^2 (colour), for $0.10 < z < 0.15$ (left) and $0.60 < z < 0.70$ (middle).

As stated previously, the here performed studies are based on simulations with the field strength of the ECCE superconducting solenoid set to 1.4 T. An alternative configuration, where the field strength is set to 3.0 T has also been considered. The influence of the higher magnetic field strength is illustrated in Figs. 8 and 9. As Figs. 4–5, 8 shows the uncertainties in the A_1 asymmetry as a function of the kinematic coverage in x_B (x axis) and Q^2 (colours). Here, the results for 18×275 GeV^2 and one bin in hadron fractional energy $0.10 < z < 0.15$ are shown. Comparing the 1.4 T setting (first panel) and the 3.0 T setting (second panel), it can be seen that the 3.0 T configuration allows for a similar kinematic coverage as the 1.4 T configuration. The observed behaviour is similar in all of the z bins. Additional information is provided in Fig. 9, which shows the ratio of the statistical uncertainties in the asymmetry for the 1.4 T and 3.0 T configuration for $0.10 < z < 0.15$ (left) and $0.60 < z < 0.70$ (middle). The low-z bin is in general populated by low-energetic hadrons. Since these are more likely to be deviated out of the detector acceptance by higher magnetic fields, the ratio of the uncertainties is on average below 1.0 for this low-z bin. A higher-z region, depicted in the middle panel, illustrates the fact that the higher-energetic hadrons are less deviated by a higher magnetic field, resulting in an average statistical-uncertainty ratio centred around 1. An increase of the ratio as a function of x_B is observed for fixed values of Q^2, a trend most clearly observed in the lower z region, though also visible for higher z values. This means that the 3.0 T configuration allows for a better coverage at larger values of x_B for fixed Q^2, apart for the highest x_B bin at fixed Q^2, where a drop of the ratio, likely linked to the lower cut on y and finite resolution, is observed.

4. Evaluation of the helicity distributions

The impact of the ECCE data on the helicity distributions is evaluated for the energy configurations 5×41 GeV^2 and 18×275 GeV^2. The procedure for the determination of the impact of the ECCE data follows that adopted in Ref. [12]. For the present study, the set of helicity distributions from Ref. [12], obtained by combining the standard data set of the global DSSV14 analysis [6] with simulated EIC inclusive DIS data at $\sqrt{s} = 45$ GeV, is used. With this set, A_1 asymmetries are generated and subsequently Gaussian smeared according to the uncertainties of the original data set (i.e., the original experimental data set and the simulated data at $\sqrt{s} = 45$ GeV). Following this, new sets of parton helicity distributions are extracted through a fit of the sets of replicated data. The impact of the here studied semi-inclusive DIS ECCE data is then evaluated by performing a reweighting of the obtained replicas, where the weight of each replicated data set is modified according to how well it reproduces the pion and kaon asymmetries from the simulated ECCE data at 5×41 GeV^2 and 18×275 GeV^2. The outcome of this reweighting represents the combined impact of the EIC inclusive and semi-inclusive DIS data.

Note that in principle one could start from the original set of DSSV14 helicity distributions. However, given the high precision of the EIC data and its partially new phase-space coverage, reweighting the original DSSV14 helicity distributions would result in a very limited number of helicity distributions in agreement with the ECCE data, and as a result it would compromise the statistical accuracy. Likewise, a cut of $x_B > 10^{-4}$ was imposed on the simulated data used in the reweighting exercise, since otherwise the number of reweighted
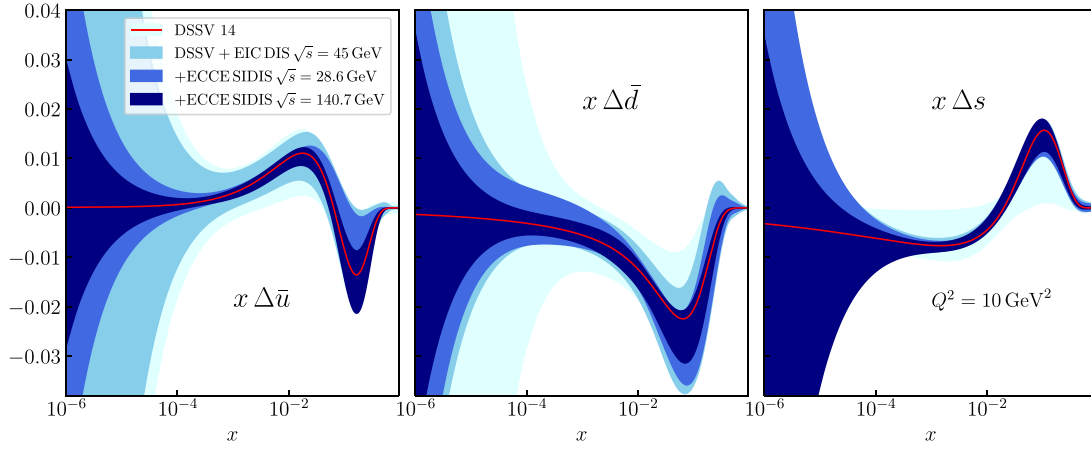
Fig. 10. Figures showing the impact of the projected ECCE semi-inclusive DIS data on the determination of the sea-quark helicity distributions for $\bar{u}$ (left), $\bar{d}$ (middle) and s (right), evaluated at $Q^2 = 10$ GeV^2. Together with the DSSV14 estimate, the uncertainty bands resulting from the fit that includes the $\sqrt{s} = 45$ GeV simulated inclusive DIS data and the reweighting with simulated ECCE semi-inclusive DIS data at $\sqrt{s} = 28.6$ GeV and $\sqrt{s} = 140.7$ GeV are presented.

replicas with non-negligible weights would be too small to obtain any reliable statistical information. The inclusion of the complete data set would require to perform a new global analysis that would presumably lead to even smaller uncertainties for the sea-quark distributions.

The impact of the ECCE data at 5×41 GeV^2 and 18×275 GeV^2 on the sea-quark helicity distributions is shown in Fig. 10. Here, the helicity distributions for $\bar{u}$, $\bar{d}$ and s as well as their uncertainty estimates are presented. The most noticeable feature after the inclusion of the ECCE semi-inclusive DIS data is the reduction of the uncertainty of $\Delta\bar{u}$ and $\Delta\bar{d}$ for $x_B < 10^{-2}$. This is driven by the data for pion production. As expected, and due to the charge factor, the $\bar{u}$ distribution is better constrained than that of $\bar{d}$. Note that the impact at $x_B < 10^{-4}$ is a consequence of the chosen parameterisation of the distributions.

5. Summary and outlook

The evaluation of the measurement of double-spin asymmetries in semi-inclusive DIS using the ECCE detector has been presented for pion and kaon production. The study shows that the ECCE design is well suited for the measurement of such asymmetries and for the subsequent extraction of parton helicity distributions. Firstly, the resolution of the ECCE detector is such that the smearing of kinematic variables is limited. Secondly, the design provides a good acceptance, allowing for the measurement of asymmetries that already without corrections reflect closely the generated asymmetries. Furthermore, the envisioned detector provides a broad kinematic coverage in x_B, Q^2 and z, aided by the possibility to vary the beam energies. In turn, the broad kinematic coverage, down to $x_B = 10^{-4}$, and a high precision are essential to constrain the helicity distributions, in particular the sea-quark and gluon helicity distributions at low x_B, which so far remain largely unconstrained.

Declaration of competing interest

The authors declare that they have no known competing financial interests or personal relationships that could have appeared to influence the work reported in this paper.

Acknowledgements

References

[1] D. de Florian, R. Sassot, M. Stratmann, W. Vogelsang, Evidence for polarization of gluons in the proton, Phys. Rev. Lett. 113 (2014) 012001, http://dx.doi.org/10.1103/PhysRevLett.113.012001, URL https://link.aps.org/doi/10.1103/PhysRevLett.113.012001.

[2] T. Sjostrand, S. Mrenna, P.Z. Skands, PYTHIA 6.4 physics and manual, J. High Energy Phys. 05 (2006) 026, http://dx.doi.org/10.1088/1126-6708/2006/05/026, arXiv:hep-ph/0603175.

[3] R. Abdul Khalek, et al., Science requirements and detector concepts for the electron-ion collider: EIC yellow report, 2021, arXiv:2103.05419.

[4] J. Bernauer, et al., Scientific computing plan for the ECCE detector at the Electron Ion Collider, Nucl. Instrum. Meth. A 1047 (2023) 167859, http://dx.doi.org/10.1016/j.nima.2022.167859.

[5] K. Abe, et al., E143 Collaboration, Measurements of R=σ(L) / σ(T) for 0.03 < x < 0.1 and fit to world data, Phys. Lett. B 452 (1999) 194–200, http://dx.doi.org/10.1016/S0370-2693(99)00244-0, arXiv:hep-ex/9808028.

[6] D. de Florian, G.A. Lucero, R. Sassot, M. Stratmann, W. Vogelsang, Monte Carlo sampling variant of the DSSV14 set of helicity parton densities, Phys. Rev. D 100 (2019) 114027, http://dx.doi.org/10.1103/PhysRevD.100.114027, URL https://link.aps.org/doi/10.1103/PhysRevD.100.114027.

[7] D. de Florian, R. Sassot, M. Epele, R.J. Hernández-Pinto, M. Stratmann, Parton-to-pion fragmentation reloaded, Phys. Rev. D 91 (2015) 014035, http://dx.doi.org/10.1103/PhysRevD.91.014035, URL https://link.aps.org/doi/10.1103/PhysRevD.91.014035.

[8] D. de Florian, M. Epele, R.J. Hernandez-Pinto, R. Sassot, M. Stratmann, Parton-to-Kaon fragmentation revisited, Phys. Rev. D 95 (9) (2017) 094019, http://dx.doi.org/10.1103/PhysRevD.95.094019, arXiv:1702.06353.

[9] R.D. Ball, et al., NNPDF Collaboration, Parton distributions for the LHC Run II, J. High Energy Phys. 04 (2015) 040, http://dx.doi.org/10.1007/JHEP04(2015)040, arXiv:1410.8849.

[10] A. Buckley, J. Ferrando, S. Lloyd, K. Nordström, B. Page, M. Rüfenacht, M. Schönherr, G. Watt, LHAPDF6: parton density access in the LHC precision era, Eur. Phys. J. C 75 (2015) 132, http://dx.doi.org/10.1140/epjc/s10052-015-3318-8, arXiv:1412.7420.

[11] D. de Florian, M. Stratmann, W. Vogelsang, QCD analysis of unpolarized and polarized Lambda baryon production in leading and next-to-leading order, Phys. Rev. D 57 (1998) 5811–5824, http://dx.doi.org/10.1103/PhysRevD.57.5811, arXiv:hep-ph/9711387.

[12] I. Borsa, G. Lucero, R. Sassot, E.C. Aschenauer, A.S. Nunes, Revisiting helicity parton distributions at a future electron-ion collider, Phys. Rev. D 102 (2020) 094018, http://dx.doi.org/10.1103/PhysRevD.102.094018, URL https://link.aps.org/doi/10.1103/PhysRevD.102.094018.